

# An ESO/VLT survey of NIR ( $Z \leq 25$ ) selected galaxies at redshifts $4.5 < z < 6$ : constraining the cosmic star formation rate near the reionization epoch <sup>1</sup>

A. Fontana, F. Poli, N. Menci

*INAF Osservatorio Astronomico di Roma, via Frascati 33, Monteporzio, I-00040, Italy*

M. Nonino

*INAF Osservatorio Astronomico di Trieste via G. B. Tiepolo, 11, Trieste I-34131 Italy*

E. Giallongo

*INAF Osservatorio Astronomico di Roma, via Frascati 33, Monteporzio, I-00040, Italy*

S. Cristiani

*INAF Osservatorio Astronomico di Trieste via G. B. Tiepolo, 11, Trieste I-34131 Italy*

S. D'Odorico

*European Southern Observatory, Karl-Schwarzschild Strasse, Garching bei Munchen, D-85748, Germany*

## ABSTRACT

We present the results of a VLT and HST imaging survey aimed at the identification of  $4.5 < z < 6$  galaxies. In the VLT data, a set of broad and intermediate band filters has been used to select 13 high- $z$  candidates in a  $Z_{AB} \leq 25$  *mags* catalog, over an area of about 30 arcmin<sup>2</sup>. Discrimination against lower redshift interlopers (mainly early-type galaxies at high redshift and cool Galactic stars) has been done combining morphological and spectral classification. This sample has been combined with a deeper  $I_{AB} \leq 27.2$  *mags* sample obtained from the Hubble Deep Field campaigns.

The VLT final sample consists of 13 high- $z$  candidates, 4 of which are identified with high confidence as  $z > 4.5$  galaxies. The resulting integral surface density of the  $Z_{AB} < 25$  candidates at  $z > 4.5$  is in the range  $0.13 - 0.44$

---

<sup>1</sup>Based on observations obtained in service mode at the ESO VLT for the program 65.O-0445

arcmin<sup>-2</sup> and that in the highest redshift bin  $5 < z \leq 6$  is between  $0.07 - 0.13$  arcmin<sup>-2</sup>. In the two HDFs, we identify at  $I_{AB} \leq 27.2$  25 galaxies in the range  $4.5 \leq z < 5$  and 16 at  $5 \leq z \leq 6$ , corresponding to surface densities of 3.1 arcmin<sup>-2</sup> and 2 arcmin<sup>-2</sup>, respectively.

We show that the *observed*  $Z_{AB} < 25$  UV luminosity density appear to drop by about one order of magnitude from  $z \simeq 3$  to  $z \simeq 6$ . However, if we apply a threshold to obtain an absolute-magnitude limited sample, the UV luminosity density results to be roughly constant up to  $z \simeq 6$ .

We finally show that recent semi-analytic hierarchical models for galaxy formation, while predicting a nearly constant *total* UV luminosity density up to  $z \simeq 6$ , under-predict the observed UV luminosity density at  $Z_{AB} \leq 25$  and over-predicts the  $I_{AB} \leq 27.2$  one. This behaviour can be understood in term of a poor match to the slope of the UV luminosity function.

*Subject headings:* galaxies: distance and redshifts — galaxies: formation

## 1. Introduction

Current findings on the production of the stellar baryon budget of the Universe (Madau et al. 1998), have shown a complex, gradual process, spread across a considerable fraction of the cosmological lifetime, rather than confined into a preferred epoch in the past. The evolution of the rest-frame ultraviolet luminosity density can be used to trace this process: since it is produced mainly by O, B short-living massive stars, it is almost independent of the star formation history of the galaxies (Madau, Pozzetti & Dickinson 1998), but it is tied to the fraction of the current star formation rate not extinguished by dust.

Measurements of the UV luminosity density from local environment up to  $z \simeq 1$  show an increase with redshift (Lilly et al. 1996, Madau 1996, Wilson et al 2002). At the highest redshifts, where the results are often based on imaging surveys and photometric redshifts, the UV luminosity density appears to be roughly constant between  $z = 1$  and  $z \sim 4$  (Connolly et al 1997, Pascarelle et al 1998, Fontana et al. 1999, Steidel et al 1999, Lanzetta et al. 2002)

Here we focus upon the redshift interval  $z = 4.5 - 6$ , a range which marks a critical phase in the history of the Universe, when it was just emerging from the reionization epoch. Although first glances of the early Universe have been made possible from Sloan Survey, that have provided the first statistically defined sample of quasars extending up to  $z = 6.28$ , the galaxy population at these epochs is presently nearly unexplored.

Indeed it is at these very high redshifts that it is possible to set severe constraints on the physical mechanisms that drive the galaxy formation and evolution. The main goal behind the study of high redshift galaxies is the construction of a coherent picture of the physical processes that led to galaxy evolution. Within the framework of gravitational instability driven by primordial fluctuation, simple but physically motivated prescriptions have been used over the last years to describe the main processes involved (e.g. White & Frenk 1991; Cole et al. 1994,2000; Somerville & Primack 1999; Menci et al. 2002). These models are not as “tunable” as commonly believed since they can not be modified freely to match the high redshift observables without worsening the local fits (e.g. the local luminosity function or local Tully-Fisher relation). In this respect, any discrepancy between the model predictions and the observed properties reveals the lack or incorrect treatment of some fundamental processes. In this context, it is important to perform these comparisons directly at the highest redshifts, where the physical processes leading to present-day galaxies are caught in act.

Despite the obvious interest in the field, and the exciting results obtained at  $z \simeq 3$  (Steidel et al. 1996), the discovery of galaxies at  $z > 4.5$  has been so far serendipitous. There are obvious difficulties to tackle: first, the objects become progressively fainter and rarer. Second, the multicolor “drop-out” criteria used to select high- $z$  galaxies must be shifted from the UV-visual into the near-IR bands to follow the rest-frame UV. For the same reasons, the spectroscopic follow-up is progressively harder. Besides this, the number of possible interlopers increases, with early-type galaxies and late-type stars progressively entering in the selection criteria. The current statistics of high- $z$  galaxies reflects these problems. Few serendipitous objects have been identified (e.g. Spinrad et al 1998), mostly because of a large EW emission line identified as  $\text{Ly}\alpha$ , (e.g. Chen et al 1999; Hu et al. 1998, 1999, 2002). Some identification have been later disputed on the basis of deep imaging shortward of the (presumed) Lyman Limit (Chen et al 2000, Stern et al 2000). In general, the search of  $z \geq 5$  emission line galaxies has been shown to suffer from the strong contamination by OII emitters at  $z \simeq 1.4$  (Stern et al 2000). Thus, the conclusions that can be drawn from the few objects observed so far are that *a*) spectroscopy is by itself not conclusive at these redshifts to derive a firm estimate of the average cosmic star formation rate, firstly because it mostly requires the existence of a strong  $\text{Ly}\alpha$  emission line, and because of the contamination from OII emitters; and *b*) deep imaging observations are required in any case not only to select the objects but also to validate the spectroscopic identifications.

Previous color selections at  $z > 4.5$  based on the photometric redshift technique (Fontana et al. 1999, 2002) took advantage of the very deep HST North and South samples, discovering 4  $z > 5.5$  candidates in each field down to  $I_{AB} < 27.5$ . Evidence has come up for a comoving UV luminosity density at  $z \simeq 5$  lower by a factor of 5 than at  $z \simeq 3$ . However,

this estimate is based on a sample of very faint sources selected in a small area and could be strongly affected by the presence of large-scale structure in the “pencil” beams.

For this reason, we have started a relatively deep survey of galaxies selected in the Z band to search for galaxies at  $4.5 \leq z \leq 6.2$ , covering two well known fields where broad band multicolor imaging is available, namely the extended ESO Imaging Survey (EIS) Hubble Deep Field South and the NTT Deep Field. We have designed a strategy based on a combination of intermediate and broad band filters to identify high- $z$  galaxies against the increasingly large number of interlopers. We emphasize that this is not a “pre-selection” survey, but it is designed to provide by itself a reliable identification for the bulk of the galaxy population at  $z \geq 5$ . To increase the accuracy of the photometric estimate of the redshift and to minimize the presence of interlopers (mainly intermediate redshift early-type galaxies and late type stars) in our high  $z$  sample, we have included a set of intermediate band filters namely IB691, IB834 and IB915, available at the ESO/VLT FORS imager. These filters, although of intermediate width, are relatively efficient since they sample spectral regions devoid of strong sky emission lines. The adopted filter set is thus tailored to trace the peculiar spectral features of the extremely high redshift galaxies, i.e. the flat rest-frame UV continuum that even at  $z \sim 6$  can be sampled by the Z-IB915 color and the very abrupt change of the shape due to the hydrogen absorption spectral breaks by the intergalactic and interstellar medium sampled by the bluer bands.

In the following, we will adopt a  $\Lambda$ CDM cosmology with  $\Omega_\Lambda = 0.7$ ,  $\Omega = 1$  and  $H_0 = 70$  km/s/Mpc. All magnitudes will be given in the AB system.

## 2. Photometric database and the selection of the sample

The dataset that we have analyzed consists of a composite sample of optical and infrared images centered on two public deep fields: a  $16.3 \text{ arcmin}^2$  area around the ESO/NTT deep field (NDF, Arnouts et al. 1999) and a  $13.6 \text{ arcmin}^2$  area around the Hubble Deep field South (HDFS). The new data presented here have been obtained with the spectroimagers FORS1 and FORS2, at VLT-Antu and VLT-Keyun respectively, in the R, IB691, I, IB834, Gunn  $z$  and IB915 bands, and coupled with available UBV and near-IR images obtained at NTT (Saracco et al 1999, (da Costa et al 1998, Fontana et al 2000). Details of the observations are given in Table 1.

Data reduction has followed the usual steps for deep imaging surveys in dithered mode, as described for instance in Fontana et al (2000). Since fringing effects have been found to be significant in the reddest bands, we have applied a special care in masking even the faintest

objects prior to fringing removal. To account for the remaining sky residuals and for the pixel-to-pixel correlation induced by dithering, we have adopted an estimation of the noise from sky variance inside a  $3''$  diameter aperture as described in Hu et al. (1999).

In the overall  $29.9 \text{ arcmin}^2$  area common to the optical and IR observations, a photometric multicolor catalog of objects detected in the Gunn  $z$  band has been extracted following a recipe tailored to obtain accurate color photometry from ground-based images with different seeing conditions that we developed and tested on the imaging data of the K20 survey (Cimatti et al 2002). Total magnitudes and colors have been estimated by the SExtractor code (Bertin & Arnouts 1996). For relatively bright objects, both the total flux in the Gunn  $z$  images and colors have been estimated from the MAG\_AUTO magnitude. For faint objects, we have used aperture magnitudes obtained by measuring fluxes within three increasing aperture diameters of  $1''$ ,  $2''$  or  $3''$  depending on the relative distance of the nearest source. In this case, an average correction (estimated on brighter galaxies) has been applied to account for seeing differences among different bands. The choice of apertures of  $1''$ ,  $2''$  and  $3''$  has been taken on the basis of the results obtained within the K20 dataset, where we found that using apertures as large as  $3''$  (for isolated objects) still leads to an improvement in the accuracy of photometric redshifts. In the case of the present data, where the sample is deeper and the seeing of the the detection image is better than the K20  $K$  images, we verified that the results do not depend on the exact choice of the largest aperture. Indeed, we still select the same sample of  $z \geq 4.5$  candidates and obtain similar estimates of the UV luminosity densities even using catalogs based on  $2''$  apertures, although the total magnitudes of individual objects may vary up to about 0.1 mags. We limit in the following the discussion to the  $Z_{AB} < 25$  subsamples.

The selection of high- $z$  candidates has been performed using the complete multiband catalogs. The spectral features that identify high redshift galaxies are the abrupt spectral breaks due to intervening and intrinsic HI absorption and the flat rest-frame UV continuum long-ward of Lyman  $\alpha$ . In particular, the HI absorption produces flux dropouts in the V, R and even I bands as the redshift increases from  $z = 4.5$  to  $z = 6$ . The selection of high- $z$  candidates is usually done with color selection criteria sensitive to this pattern. In our case, due to the large number of filters adopted and to the relatively wide redshift range covered, we have directly applied our photometric redshift code, that is described in details in Giallongo et al (1998) and Fontana et al (2000). The only difference respect to these papers is that we have used here a set of spectral templates obtained with the Pegase 2.0 code (Fioc and Rocca-Volmerange 1997), that we have found to provide accurate redshift estimation on ground-based data sets (Cimatti et al 2002, Fontana et al 2002). As shown in Fontana et al (1999) and Fontana et al (2000), the selection of high- $z$  candidates with photometric redshifts is at least as efficient as the simple “drop-out” technique at  $z \simeq 3$ ,

and more efficient at higher  $z$ .

Potential contaminants of the selected subsample of  $z_{fit} > 4.5$  candidates might come either by early-type galaxies at  $z > 1$  (that may mimic the large spectral breaks in the optical bands) or by cool galactic stars that could mimic the main spectral features of galaxies in this redshift range, as shown by Fontana et al (2000).

The contaminations from the first class of interlopers is easy to treat with our filter set, since early-type galaxies have very bright detections in the infrared J and K bands, so that they are automatically excluded by our photometric redshift code.

The cleaning of the sample from the second kind of interlopers has been achieved following a double selection criterion, based both on morphological and spectral informations. Morphology has been taken into account using the SExtractor **CLASS\_STAR** classification parameter (Bertin 1996), that sharply classifies the objects in our samples down to  $Z_{AB} \leq 24$ . In addition, the stellar spectral library by Pickles (1998) has been used to compute the expected stellar colors in our filter sets, to provide additional spectroscopic criteria for the star-galaxy separation.

We have first obtained the exclusion of obvious bright stars from the sample removing the objects at  $Z_{AB} \leq 24$  with **CLASS\_STAR**  $\geq 0.85$ : the objects removed by this criteria are also better fitted by stellar templates. We provide a check of the reliability of this morphology-based classification in figure 1, where the best fit galactic spectrum is shown along with a best fit outcome from a library of stellar spectra for four out of the whole sample of **CLASS\_STAR**  $> 0.85$  and  $Z_{AB} \leq 24$  high redshift candidates. After this selection we found no high redshift candidate at this relatively bright magnitude cut.

In the fainter magnitude interval  $24 < Z_{AB} \leq 25$ , 16 objects have been detected by our photometric redshift code as having  $z > 4.5$ . Here an automatic classification becomes less reliable, since morphology cannot be accurately estimated at these faint levels. These candidates have been therefore inspected visually, and morphological information has been complemented with a comparison between the best fit  $\chi^2$  of the galactic template and the  $\chi^2_{STAR}$  of the stellar spectra.

From this analysis, we have singled out a “minimal” subsample of 4 sources, that represent the most robust candidates showing clear extended morphological features, self-consistently detected in more than one band. On the other hand, 3 point like sources have been excluded as having stellar full widths at half maximum in more than one band. For these objects, the spectral energy distribution is also more consistent with that predicted by the stellar library, i.e.  $\chi^2_{STAR} < \chi^2$ . The remaining 9 objects constitute the sample of candidates showing ambiguous characteristics, i.e.  $\chi^2_{STAR} > \chi^2$  but compact morphology or

extended morphology but  $\chi_{STAR}^2 < \chi^2$ .

The spectral energy distribution of 12 out of our 13 candidates are shown for illustrative purpose in Fig.2, together with their best fit galaxy templates. The crucial role played by intermediate band filters is evident especially in those cases where only upper limits or strongly uncertain values are available for the NIR J,K bands. In this way it is possible to sample the main features of this spectra, i.e. the strong drop short-ward the Lyman series absorption and the quite flat behavior long-ward the same wavelength with an accuracy sufficient to discriminate between galaxies at  $4.5 < z < 5$  and  $5 < z < 6$ .

In the following we will also use the photometric redshift sample of the WFPC2–HDFN and WFPC2–HDFS fields, presented in Fontana et al (2000) and Fontana et al (2003), to select  $z > 5$  galaxies at a deeper threshold of  $I_{AB} \leq 27.2$ . For the HDFS, the sample has been obtained from a new optical–IR catalog that uses ultra-deep IR observations obtained with VLT–ISAAC. The catalog extraction procedure is described in Vanzella et al (2001), while the final optical–IR photometric redshift catalogs are presented in Fontana et al (2003). In both cases, we will adopt a  $I_{AB} \leq 27.2$  selection criterion that ensures a small level of systematics in the estimated magnitudes (Vanzella et al 2001). Combining the two HDFs samples, we identify at  $I_{AB} \leq 27.2$  25 galaxies in the range  $4.5 \leq z < 5$  and 16 at  $5 \leq z \leq 6$ . A large variance still exists between the statistics in the two field, with 17 (4) objects at  $4.5 \leq z < 5$  ( $z > 5$ ) in the HDFS, against 8 (12) in the HDFN.

A close up of the HDFS  $z > 5$  candidates is shown in Fontana et al (2003).

We note that the new WFPC2–HDFS catalog leads to major changes respect to the one used in Fontana et al (1999), that was based on the Stony–Brook catalog (Lanzetta et al 2002). In particular, three clear candidates at  $z \geq 5.5$  that were absent in the previous catalog have been found at  $I_{AB} \leq 27.2$ . We found that this comes from a systematic underestimate of the magnitudes at the faint levels in the Stony–Brook catalog, that prevented these objects from being included in the  $I_{AB}$  selected catalog.

The resulting integral surface density of the  $Z_{AB} < 25$  candidates at  $z > 4.5$  is in the range  $0.13 - 0.44 \text{ arcmin}^{-2}$  and that in the highest redshift bin  $5 < z \leq 6$  is between  $0.07 - 0.13 \text{ arcmin}^{-2}$ . It should be emphasized that the stellar contamination of candidates at  $z > 4.5$  ranges from a minimum of about 20% to a maximum of 75%. Thus any estimate of the surface density of very high  $z$  protogalaxies should include a careful analysis of the contamination by the faint stellar population present in a given survey. In the two HDFs, the resulting surface densities at  $I_{AB} \leq 27.2$  is of  $3.1 \text{ arcmin}^{-2}$  and  $2 \text{ arcmin}^{-2}$ , respectively.

Our lower and upper limits on the observed number densities at  $Z_{AB} < 25$  and  $5 < z \leq 6$  are 2–4 times higher than those predicted in the redshift range  $5.5 < z \leq 6.5$  by Yan et al

(2002), who assumed that the shape of luminosity function does not change from  $z \simeq 3$  to  $z \simeq 6$ . The slightly higher value that we find is mainly due to the lower normalization adopted by Yan et al (2002), who chose to adopt 1.37 galaxies arcmin<sup>-2</sup> at  $I_{AB} \leq 27.2$ , while we detect 2 galaxies arcmin<sup>-2</sup>, and to the slightly lower redshift bin that we select. We also note that the ratio between the number densities measured at  $Z_{AB} \leq 25$  and at  $I_{AB} \leq 27.2$  is within a factor of two of that predicted by Yan et al (2002), which may suggest that the slope of the UV luminosity function remains indeed unchanged from  $z \simeq 3$  to  $z \simeq 6$ .

### 3. Evaluating the observed and predicted UV luminosity density

We present in this section the UV luminosity density resulting from our samples, using the usual  $1/V_{max}$  formalism as described in Poli et al (2001). Given the good agreement between data of the two fields, we compute the average UV luminosity density (LD hereafter) of the total sample including both NDF and HDFS objects, in the two redshift bins  $4.5 < z \leq 5$  and  $5 < z < 6$ .

In both bins, the uncertainties due to possible stellar contamination are bracketed by the two triangles in the same redshift bin. The upward triangles represent the estimate derived from our minimal sample. The downward ones are derived from the total sample. Error bars are simply computed from Poisson statistics on the total number of galaxies in each bin following the recipe in Geheerls (1986) in the case of small numbers.

Although we are focusing on the two highest redshift bins, we have also computed the luminosity density at  $2.5 < z < 4.5$ , to show its evolution on a complete  $Z < 25$  sample. Again, photometric redshifts are estimated from the multiband observations, and stars have been excluded with a morphological and spectral classification similar to the one described above.

The *observed* quantities are shown in Fig 3a. As in Fontana et al. (1999), and at variance with other works, we have not corrected the observed values of the UV LD for incompleteness or extinction, but we explicitly show the differential effects of the inclusion of a magnitude limit and different dust extinction curves on the theoretical expectations that we will discuss below.

To complement these observations, we present in Fig. 3b the same quantities derived in the WFPC2 HDFN and HDFS  $I_{AB} \leq 27.2$  samples.

At face value, the resulting picture is that the *observed* UV LD at  $Z_{AB} < 25$  remains about constant in the redshift interval  $2.5 < z < 4.5$  to values of the order of  $10^{26}$  erg s<sup>-1</sup>



$\text{Hz}^{-1} \text{Mpc}^{-3}$  and then decreases by a factor of 10 reaching  $10^{25}$  (average between our minimal and total sample of  $5 < z < 6$  candidates).

However, the comparison between the UV LD values computed in this way at different redshifts is prone to several biases. First, the  $Z < 25$  or  $I_{AB} \leq 27.2$  selection criterion results in a progressively brighter cutoff to the luminosity function at increasing redshifts. Second, the rest-frame wavelength span by the Gunn  $z$  band ranges from  $2250 \text{ \AA}$  at  $z \simeq 3$  to  $1300 \text{ \AA}$  at  $z \simeq 6$ , which may introduce color-dependent selection effects when computing the UV LD in the lowest redshift bins. The correction of both effects is uncertain, since it depends on the (largely unknown) shape of the luminosity function and color properties of the high- $z$  galaxies.

In order to deal with these systematics in a clean way, we reproduce them in the theoretical predictions as we will describe below. A coarse correction of the varying luminosity cutoff is possible if we compute the UV LD limited at the faintest absolute magnitude of the highest  $z = 5 - 6$  sample, i.e. at limiting fluxes of  $1.2 \times 10^{29} \text{ erg/s}$  and  $3.6 \times 10^{28} \text{ erg/s}$  (corresponding to  $M_{1400} \leq -19.8, -21.1$ ) in the  $Z$  and  $I$  selected samples, respectively. The corresponding values are shown with empty symbols in both figures. The resulting picture is that the UV luminosity density of the brightest galaxies results to be roughly constant from  $z \simeq 3$  to  $z \simeq 6$ .

The values of the UV luminosity densities are given in Tab.2.

## 4. Discussion

In this work we have presented the results of a pilot survey aimed at detecting  $z > 4.5$  galaxies with deep multicolor images. The key features of our approach are *a)* the use of an extended set of broad (UBVRIZJK) and intermediate band ( $\Delta\lambda \simeq 400 \text{ \AA}$ ) filters centered at  $6900$  and  $8340 \text{ \AA}$ , *b)* the adoption of conservative thresholds on the S/N for object detection and *c)* the application morphological and spectral criteria: all these aspects improve the estimates of the redshifts, and help exclude or minimize the number of lower  $z$  interlopers. When applied to the present data set, these criteria make it possible to reject all the brightest interlopers, that would dominate the LD, and to select a “minimal” sample of 4 high-confidence candidates at  $z > 4.5$ , and a sample of 9 additional candidates where the stellar contamination is uncertain. This ambiguity depends on the relative depth of our data set: it is well within the possibilities of red-enhanced imagers at 8-m class telescope or of ACS to extend this kind of analysis 1-2 magnitudes fainter, so that the stellar contamination to the LD can be lowered by a large amount, as in the case of deeper but smaller WFPC2-

HDF data that we present here.

Even with this ambiguity, the two selected datasets constrain the  $z > 4.5$  UV LD with sufficient accuracy to show that the *observed*  $Z_{AB} < 25$  UV LD drops by about one order of magnitude from  $z \simeq 3$  to  $z \simeq 6$ . This drop is largely due to the progressively brighter cutoff in the rest frame luminosity function: if we correct for this incompleteness, the UV LD appears to be roughly constant from  $z \simeq 2.5$  up to  $z \simeq 6$ .

The present results are apparently in contrast with recent findings by Lanzetta et al (2002), who make use of the same WFPC2–HDF data and apply photometric redshifts, that claim the global SFR to steadily increase up to  $z = 12$ . Unfortunately, the overall approach and techniques adopted are so different that it is difficult to make a clean comparison. First, we note that the use of wide aperture magnitude and the adoption of a much higher S/N threshold to the catalog strongly reduce the systematics in the WFPC2 data induced by surface brightness dimming, that otherwise require the complex and model–dependent correction applied by Lanzetta et al (2002). Besides, we draw our conclusions from a homogeneous sample, that includes only objects selected down to the same absolute magnitude limit, rather than correcting for the incomplete coverage of the luminosity function, as done by Lanzetta et al (2002). Finally, the photometric redshift distribution obtained by Lanzetta et al (2002) is markedly different from our own, and peaks at  $z \simeq 0$ , a factor that may lead to an overestimate of the faint end of the SFR distribution function that is used to correct the high- $z$  data. Despite all these differences, it is to be noted that the two results are still consistent when the more conservative estimate of Lanzetta et al (2002) is compared with our data in the appropriate redshift range  $z \simeq 3$  to  $z \simeq 6$ : given the overall uncertainties both analyses suggest that UV LD is roughly constant in this redshift range.

The question that naturally arises is whether a constant UV LD up to  $z \simeq 6$  may be compatible with the hierarchical scenario of galaxy formation. To discuss this point, we present in both panels of fig. 3 the UV LD predicted by the CDM semianalytic model described in Menci et al. (2002). This model is based on the Cole et al (2000) recipes, with an additional improved treatment of aggregation of satellite galaxies in common DM haloes. We first show that the *total* SFR derived from this model (thin solid lines) is nearly constant from  $z \simeq 2$  to about  $z \simeq 5$ , and then fades by only a factor about 5 at  $z = 6$ .

To allow a fair comparison with our data, we have applied the effects of magnitude limit cut and dust extinction directly to the theoretical model. The effect is shown by the thick solid lines in Fig3a and Fig3b. The shaded area show the possible effects of dust extinction, ranging from no dust (upper lines) to SMC-like extinction curve (lower lines). Please note that the inclusion of dust correction effects in the theoretical model decreases the average UV LD respect to the unextincted amount. It appears that while the CDM model broadly

encompasses the observed values, it progressively under-predicts the LD observed in the bright  $Z_{AB} < 25$  sample, while over-predicts the LD observed in the faintest  $I_{AB} < 27.2$  sample. This behavior can be understood in term of a poor match to the slope of the UV luminosity function. At the brightest magnitudes, the CDM model under-predicts the number of bright sources, while it over-predicts the number of fainter sources dominating the deeper sample. This is analogous to what already found at  $z \simeq 3$  and confirms a general trend of this version of CDM models to under-predict the amount of star-formation rate in high redshift massive objects (Somerville and Primack 2001, Poli et al 2001 and Menci et al 2002, Cimatti et al 2002).

The origin of this discrepancy is likely tied to the lack or to the oversimplified treatment of fundamental physical process. Indeed, we remark that the basic recipes adopted in this model already concur to enhance the SFR in high redshift massive objects, and that these aspects are further boosted with respect to the models that we used in Fontana et al (1999). The star formation rate is computed as  $\dot{M}_* = M_g/\tau_*$ , where  $M_g$  is the amount of cool gas and the time-scale  $\tau_*$  is proportional to the dynamical time  $\tau_{dyn}$  and to the galaxy circular velocity  $V_c$  as  $\tau_* = \epsilon_*^{-1} \tau_{dyn} (V_c/200 \text{ km/s})^{\alpha_*}$ . Since both  $M_g$  and  $1/\tau_{dyn}$  increase with redshift, and  $\alpha_* = -1.5$ , these models naturally predict that the star-formation rate increases with redshift (for a given galaxy mass), and is more efficient in massive galaxies (at a given redshift). In addition, feedback effects are also a strong function of  $V_c$ , since they scale as  $(V_c)^{-5.5}$ , and again strongly favor the more massive objects. These basic recipes, combined with the effects of the biased process of galaxy formation induced by hierarchical merging, already conspire to boost at high  $z$  the SFR in massive objects, with respect to the less massive one.

In the present context, it is not possible to flatten the high- $z$  luminosity function by simply changing the free parameters of the model, since one rapidly worsens the fit to the local observables (Cole et al 2000).

Other physical processes that are important in the high- $z$  Universe are not included in our model. On the one hand, mechanical and ionizational feedback on the intergalactic medium by early galaxy and QSO formation is not included in our rendition, a process that is expected to quench the SFR in low mass objects and hereby to flatten the low luminosity side of the LF. On the other hand, molecular cooling is efficient at high  $z$  and not included here. Another possibility that has been proposed is that the starburst efficiency increases during major mergers. These “starburst” models are known to increase the bright side of the LF at  $z = 3 - 4$  (Somerville and Primack 1999), but require new additional free parameters to be introduced in the models, and may become less efficient at  $z > 5$ , when major merging events are very rare. The challenge of the next years is to include all these processes in a

self consistent picture that reproduce the high- $z$  observables.

The VLT data used in this work have been mostly obtained in the framework of the proposal 65.O-0445: we are grateful to the VLT operators and scientists that have performed the observations in service mode. The Gunn  $z$  observations of the NDF have been obtained during the Science Verification Phase of FORS2-VLT. UBV and IR images of the HDFS have been obtained by the EIS survey. The UBV observations of the NDF were performed in SUSI-2 guaranteed time of the Observatory of Rome in the framework of the ESO-Rome Observatory agreement for this instrument.

We thank the referee, R. Windhorst, for careful reading of the manuscript and useful comments.

## REFERENCES

- Bertin, E., Arnouts, S., 1996, A&AS, 117, 393 379, 440
- Chen, H.-W., Lanzetta, K. M., Pascarelle, S., 1999, Nature 398, 586
- Chen, H.-W., Lanzetta, K. M., Pascarelle, S., Yahata, N. 2000, Nature 408, 562
- Cimatti, A., Mignoli, M., Daddi, E., Pozzetti, L., Fontana, A., Saracco, P., Poli, F., Renzini, A., Zamorani, G., Broadhurst, T., Cristiani, S., D’Odorico, S., Giallongo, E., Gilmozzi, R, 2002, A&A, 392, 395
- Cole, S., Aragon-Salamanca, A., Frenk, C.S., Navarro, J.F., Zepf, S.E. 1994, MNRAS, 271, 781
- Cole, S., Lacey, C., Baugh, C., Frenk, C., 2000, MNRAS, 319, 168
- Connolly, A. J., Szalay, A. S., Dickinson, M., SubbaRao, M. U., & Brunner, R. J. 1997, ApJ, 486, L11
- da Costa, L. N. et al 1998, A&A subm, astro-ph/9812105
- Fioc, M., Rocca-Volmerange, B., 1997, A&A 326, 950
- Fontana, A., Menci, N., D’Odorico, S., Giallongo, E., Poli, F., Cristiani, S., Moorwood, A., Saracco, P. 1999, MNRAS, 310, L27
- Fontana, A., D’Odorico, S., Poli, F., Giallongo, E., Arnouts, S., Cristiani, S., Moorwood, A., Saracco, P. 2000, AJ, 120, 2206
- Fontana, A., Vanzella, E., Cristiani, S., Giallongo, E., Arnouts, S., D’Odorico, S., Donnarumma, I., Poli, F., Saracco, P., 2003, AJ, in preparation

- Gehrels, N., 1986, *ApJ*, 303, 336
- Giallongo, E., D’Odorico, S., Fontana, A., Cristiani, S., Egami, E., Hu, E., McMahon, R. G. 1998, *AJ*, 115, 2169
- Hu, E., Cowie, L. L., McMahon, R. G., 1998, *ApJ*, 502, L99
- Hu, E., McMahon, R. G., Cowie, L. L., 1999, *ApJ*, 522, L9
- Hu, E., Cowie, L. L., McMahon, R. G., Capak, P., Iwamuro, F., Kneib, J.-P., Maihara, T., Motohara, K., 2002, *ApJ*, 568, L75; Erratum: 2002, *ApJ* 576, L99 264, 201
- Lanzetta, K., M., Yahata, N., Pascarelle, S., Chen, H., Fernandez-Soto, A., 2002, *ApJ*, 570, 492
- Lilly, S., J., Le Fevre, O., Hammer, F., Crampton, D., 1996, *ApJ* 460, L1
- Madau, P., Pozzetti, L., Dickinson, M. E., 1998, *ApJ*, 498, 106
- Menci, N., Cavaliere, A., Fontana, A., Giallongo, E., Poli, F., 2002, *ApJ* 575, 18
- Pascarelle, S.M., Lanzetta, K.M., Fernandez-Soto, A., 1998, *ApJ* 508, L1
- Pickles, A. J., 1998, *PASP*, 110, 863
- Poli, F., Menci, N., Giallongo, E., Fontana, A., Cristiani, S., & D’Odorico, S. 2001, *ApJ*, 551, L45; erratum: *ApJ*, 551, L127
- Saracco, P., D’Odorico, S., Moorwood, A., Buzzoni, A., Cuby, J.-G., Lidman, C. 1999, *A&A*, 349, 751
- Somerville, R.S., & Primack, J.R. 1999, *MNRAS*, 310, 1087
- Spinrad, H., Stern, D., Bunker, A., Dey, A., Lanzetta, K. Yahil, A., Pascarelle, S., Fernandez-Soto, A., 1998, *AJ*, 116, 2617
- Steidel, C. C., Giavalisco, M., Pettini, M., Dickinson, M., Adelberger, K. L. 1996, *ApJ*, 462, L17
- Steidel, C. C., Adelberger, K. L., Giavalisco, M., Dickinson, M., & Pettini, M. 1999, *ApJ*, 519, 1
- Stern, D., Eisenhardt, P., Spinrad, H., Dawson, S., van Breugel, W., Dey, A., de Vries, W., Stanford, S. A., 2000a, *Nature*, 408, 560
- Stern, D., Bunker, A., Spinrad, H., Dey, A., 2000b, *ApJ* 537, 73
- Vanzella, E., Cristiani, S., Saracco, P., et al 2001, *AJ* 122, 2190
- White, S. & Frenk, C. S. 1991, *ApJ* 379, 52
- Wilson, G., Cowie, L. L., Barger, A. J., Burke, D. J., 2002, *AJ*, 124, 1258

Yan, H., Windhorst, R.A., Odewhan, S. C., Cohen S. H., 2002, ApJ, 580, 725

Table 1: Summary of the Observational Data

Filter	NTT DF			HDFS		
	Instrument	Seeing	mag. lim. <sup>(1)</sup>	Instrument	Seeing	mag. lim. <sup>(1)</sup>
U	NTT-SUSI2	0.97	27.5	NTT-SUSI2 <sup>(2)</sup>	1.02	28.3
B	NTT-SUSI2	1.26	28	NTT-SUSI2 <sup>(2)</sup>	0.92	28.0
V	NTT-SUSI2	1.12	27.6	NTT-SUSI2 <sup>(2)</sup>	1.04	28.1
R	VLT-FORS1	0.88	28.4	VLT-FORS1	0.86	27.9
IB691	VLT-FORS1	0.55	28.1	VLT-FORS1	0.68	27.8
I	VLT-FORS1	0.81	27.4	VLT-FORS1	0.65	27.2
IB834	VLT-FORS1	0.63	27.2	VLT-FORS1	0.82	26.6
z	VLT-FORS2 <sup>(2)</sup>	0.65	27.1	VLT-FORS1	0.65	26.2
IB913	VLT-FORS2 <sup>(2)</sup>	0.65	26.4	-	-	-
J	NTT-SOFI <sup>(2)</sup>	0.77	25.7	NTT-SOFI <sup>(2)</sup>	1.04	25.8
H	-	-	-	NTT-SOFI <sup>(2)</sup>	1.03	24.43
K	NTT-SOFI <sup>(2)</sup>	0.7	25.1	NTT-SOFI <sup>(2)</sup>	1.06	24.87

(1): Computed in the AB system, at  $1\sigma$ , in 2 arcsec. Limiting magnitudes have been estimated from the photometric catalogs used in the paper, and defined as the typical value at which  $\Delta m = 1.08/3$ .

(2): Public data, from <http://www.eso.org>

Table 2: Measured UV luminosity density at  $z \geq 2.5$

Redshift	VLT: $Z_{AB} \leq 25$		HDFs: $I_{AB} \leq 27.2$	
	$\log \rho_{1400}(\text{erg s}^{-1} \text{ Hz}^{-1} \text{ Mpc}^{-3})$		$\log \rho_{1400}(\text{erg s}^{-1} \text{ Hz}^{-1} \text{ Mpc}^{-3})$	
	$Z_{AB} \leq 25$	$M_{1400} \leq -21.1$	$I_{AB} \leq 27.2$	$M_{1400} \leq -19.8$
3	26.07	25.36	26.22	26
4	25.94	25.5	25.74	25.47
4.75	$25.52 \div 25.74^{(1)}$	$24.61 \div 25.31^{(1)}$	25.78	25.65
5.5	$24.73 \div 25.26^{(1)}$	$24.73 \div 25.26^{(1)}$	25.43	25.43

(1): The two numbers correspond to the minimal and whole sample, as defined in the text.

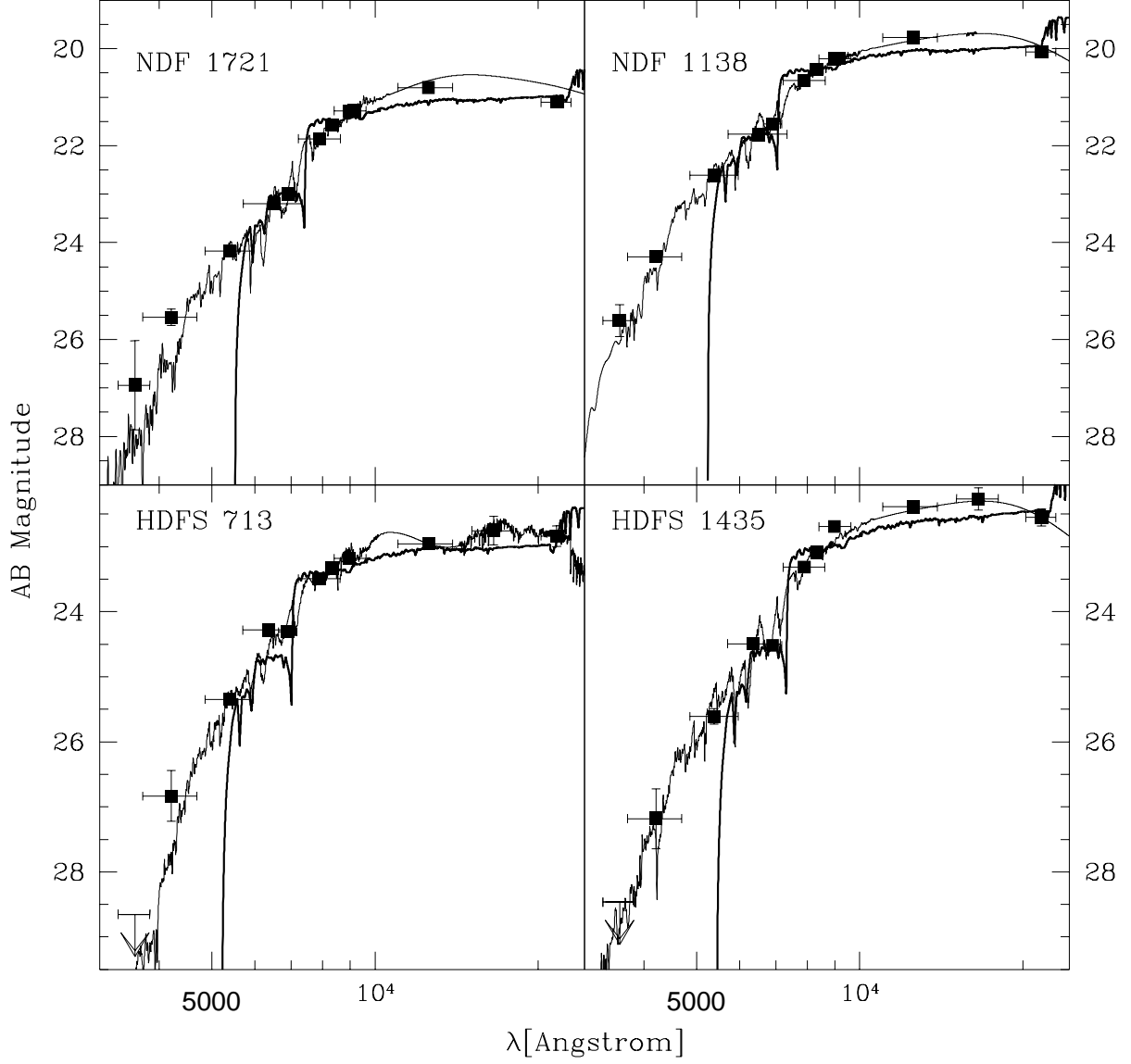


Fig. 1.— Best fit spectral templates from the Rocca-Volmerange library (thick line) and from a library of stellar spectra (thin line) for a sample of  $\text{CLASS\_STAR} > 0.85$  and  $Z_{AB} \leq 24$  high redshift candidates.



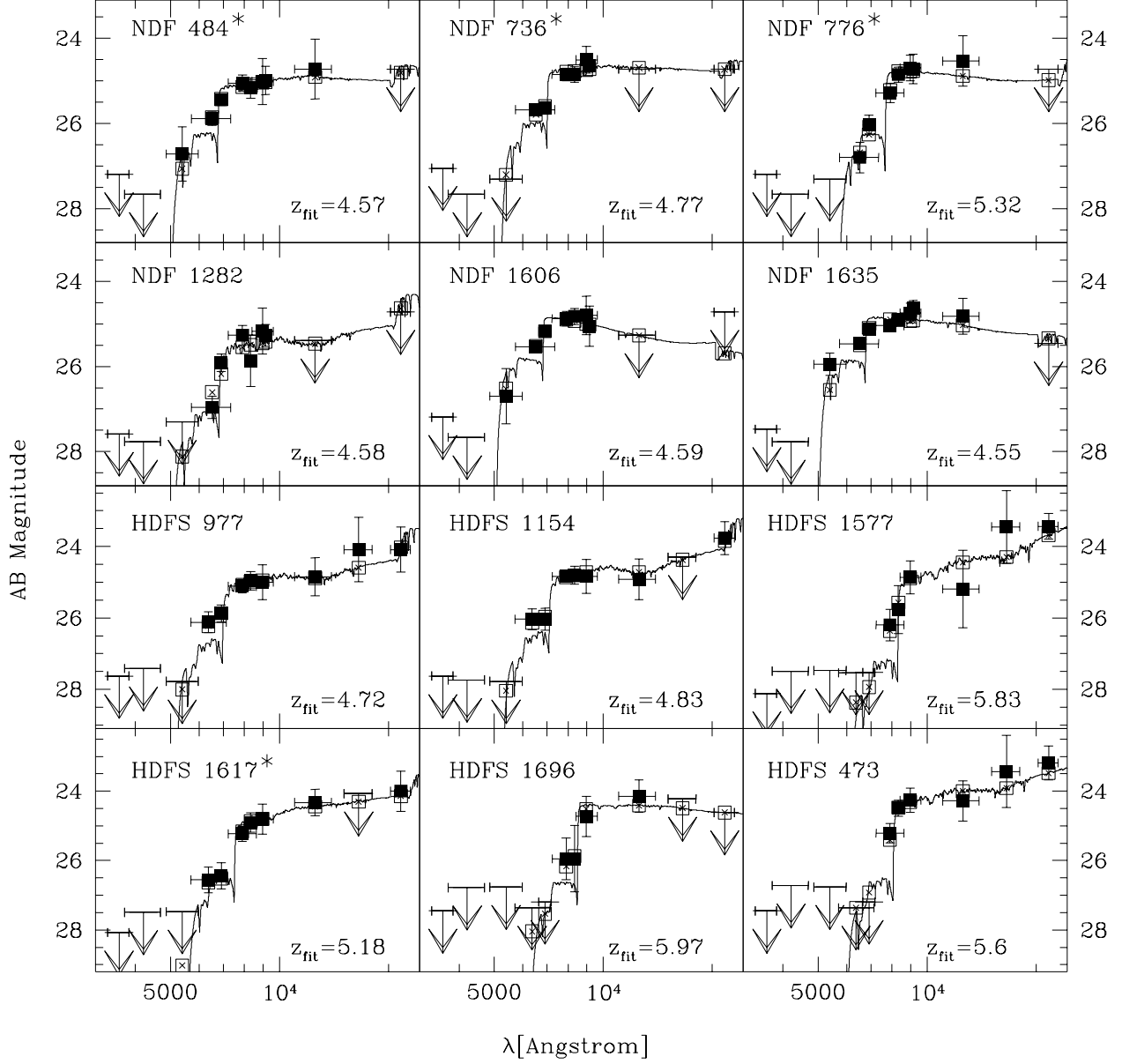


Fig. 2.— Best fit spectral templates for 12 out of our 13 high redshift candidates. Filled squares are measured AB magnitudes, 1 sigma upper limit values are displayed as downwards arrows. Empty squares represent the mean value of the spectrum inside the filters. Objects with asterisk belong to the “minimal” sample.

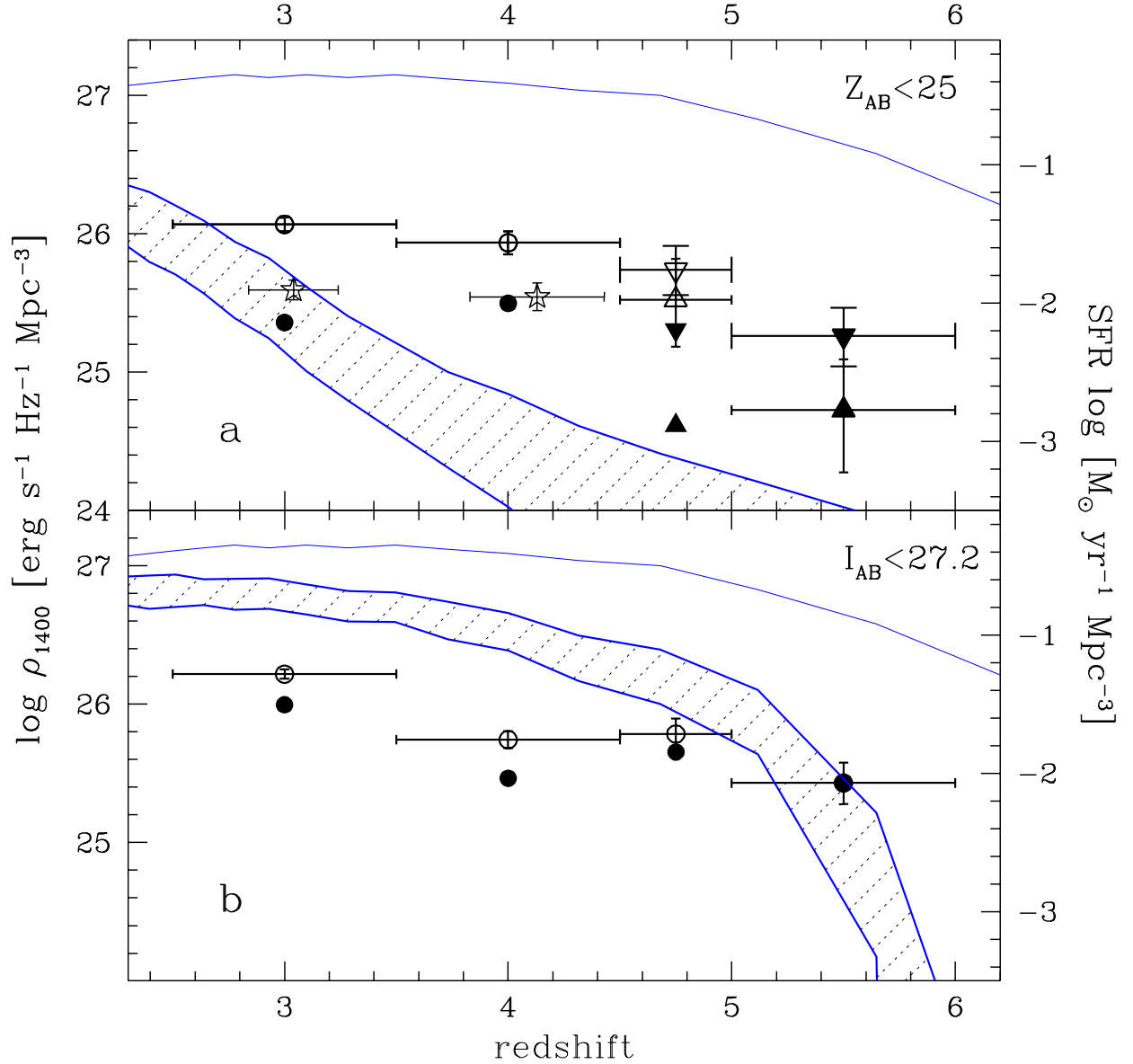


Fig. 3.— Observed and predicted UV luminosity densities as a function of redshift. **a)** Data from our  $Z_{AB} \leq 25$  survey. Upward triangles represent our estimates from the minimal sample, downward triangles from the whole sample (see text for details). Empty points represent the observed quantities. Filled symbols are the same quantities computed in a homogeneous sample that includes only objects down to the faintest absolute magnitude of the highest  $z = 5 - 6$  sample (see text for details). Empty stars represent the values from the Steidel et al. 1999 spectroscopic sample of galaxies at  $R \leq 25$  shown for comparison. The continuous curves delimiting the shaded area represent the predictions at  $Z_{AB} \leq 25$  by our fiducial model adopting different extinction curves for dust absorption. The thin curve shows the total UV (unobscured) luminosity density associated with the total star formation rate of the fiducial model. **b)** UV LD from the WFPC2 HDF-N/S sample of  $I \leq 27.2$  galaxies. Symbol meaning and predicted curves are as in a)